Toward Real-Time Simulation of Physics Based Lithium-Ion Battery Models

Venkat R. Subramanian,*,z Vijayasekaran Boovaragavan,** and Vinten D. Diwakar**

Department of Chemical Engineering, Tennessee Technological University, Cookeville, Tennessee 38505, USA

Recent interest in lithium-ion batteries for electric and hybrid vehicles, satellite, defense, and military applications has increased the demand on the computational efficiency of lithium-ion battery models. This paper presents an effective approach to simulate physics based lithium-ion battery models in real-time (milliseconds) for simulation and control in hybrid environments. The battery model used for the simulation is derived from the first principles as an isothermal pseudo two-dimensional model with incorporation of concentrated solution theory, porous electrode theory, and due consideration for the variations in electronic/ionic conductivities and diffusivities using the Bruggmann coefficient.
© 2007 The Electrochemical Society. [DOI: 10.1149/1.2776128] All rights reserved.

Mathematical modeling of lithium-ion batteries involves the specification of the dependant variables of interest (e.g., solution phase potential, solution phase concentration) and the first-principles-based derivation of governing equations for these dependant variables (based on actual physics of the battery system) with specification of boundary and initial conditions. Doyle et al.[1] developed a model for a lithium-ion sandwich that consists of a porous electrode, separator and a current collector. This model is based on concentrated solution theory,[2] and this important effort paves the way for number of similar model developments because this model is general enough to incorporate further developments in a battery system.[3-10]

Botte et al.[11] made an extensive review on mathematical modeling of secondary lithium batteries. A review of mathematical models of lithium and nickel battery systems developed by White's research group and other groups at the University of South Carolina are discussed in detail elsewhere.[12] Another review of models for predicting the cycling performance of lithium-ion batteries can be found in the literature.[13] Table I shows a standard pseudo-2D (two-dimensional) isothermal model for lithium-ion battery.[6] The boundary and initial conditions required to solve this system of equations are given in Tables I and II. The parameters used for the entire simulation are given in Table III. The corresponding schematic of a discretization stencil are shown in Fig. 1a and b, respectively.

For analysis and control of lithium-ion batteries in hybrid environments (with a fuel cell, capacitor, or electrical components), there is a need to simulate state of charge, state of health, etc., of lithium-ion batteries in real time (milliseconds). Rigorous physics based models take up to few minutes to simulate discharge curves depending on the solver, routines, computers, etc. Circuit or empirical models (based on the past data) can be simulated in real time. However, these models fail at various operating conditions, and use of these models might cause abuse or under utilization of electrochemical power sources. This paper presents a novel approach that helps us simulate physics based lithium-ion battery models in real time without compromising on accuracy.

Model simplification for any modeling system depends on the model complexity and order of the models. In the literature, order reduction based on volume-averaging, Liapunov–Schmidt technique, etc., has been illustrated for various systems, including monolith reactors.[14-17] Even classical perturbation techniques can help in simplifying the models and, hence, the number of equations to be solved. However, to our knowledge these methods have been applied only for models in which the independent variable, x for ex-

ample, varies between 0 and 1 or L (constant physical properties across the entire domain of interest). Lithium-ion batteries have three regions of different physical properties with different number of equations in each region (positive electrode/separator/negative electrode). In addition, standard order reduction techniques require a parameter (for example, aspect ratio, time constant, etc.) based on which the order of PDEs is reduced [for example, 2D to 1D (one-dimensional) or 1D PDE to ODE].

In this paper, we present the progress we have made in simulating lithium-ion battery models in real time. The math involved in simplifying lithium-ion battery models is too complicated to be reported in one paper. This paper only provides the basic concept and encouraging results, the future publications will present further details. The results obtained by using the reduced-order models are compared to the rigorous numeric simulation and validated.

Real-time simulation of lithium ion battery models.— Given the number of space discretized equations involved, real-time simulation of the lithium-ion battery model is impractical as of today. Real-time optimization and feedback control of a sensitive lithium-ion battery, where the health of the battery is vital to the very operation of the device, requires quick-solving models that give an accurate account of the battery variables. The full physics model described in Table I is therefore not the best candidate for real-time optimization and control. To facilitate real-time simulation, more than one mathematical concept has to be used. In the present study volume averaging, approximation methods and intuition based simplification of the variables are used.

Proof of concept; simple case.— Consider the case of uniform current distribution, the electrolyte concentration governing equations in the three regions are[6]

$$\epsilon_p \frac{\partial c}{\partial t} = D \epsilon_p^{\text{bruggp}} \frac{\partial^2 c}{\partial x^2} + a_p(1 - t_+)j_p \qquad [1]$$

$$\epsilon_s \frac{\partial c}{\partial t} = D \epsilon_s^{\text{bruggs}} \frac{\partial^2 c}{\partial x^2} \qquad [2]$$

$$\epsilon_n \frac{\partial c}{\partial t} = D \epsilon_n^{\text{bruggn}} \frac{\partial^2 c}{\partial x^2} + a_n(1 - t_+)j_n \qquad [3]$$

j_n and j_p are the pore wall flux at the negative electrode and positive electrode, respectively, and for uniform current distribution they are given by

$$j_n = \frac{I}{a_n F l_n} \quad \text{and} \quad j_p = \frac{I}{a_p F l_p} \qquad [4]$$

Equations 1-3 are rewritten in dimensionless form as follows

Table I. Governing equations for a lithium-ion battery.

Region	Eq. no.	Governing equations	Boundary conditions
Positive electrode	1	$\epsilon_p \partial c / \partial t = D_{\text{eff,p}} \partial^2 c / \partial x^2 + a_p(1 - t_+)j_p$ initial condition $\quad c\|_{t=0} = c_0$	$-D_{\text{eff,p}} \partial c / \partial x\|_{x=0} = 0$ and $\quad -D_{\text{eff,p}} \partial c / \partial x\|_{x=l_{p,-}} = -D_{\text{eff,s}} \partial c / \partial x\|_{x=l_{p,+}}$
	2	$-\sigma_{\text{eff,p}} \partial \Phi_1 / \partial x - \kappa_{\text{eff,p}} \partial \Phi_2 / \partial x + 2\kappa_{\text{eff,p}} RT / F(1 - t_+)\partial \ln c / \partial x = I$	$-\kappa_{\text{eff,p}} \partial \Phi_2 / \partial x\|_{x=0} = 0$ and $-\kappa_{\text{eff,p}} \partial \Phi_2 / \partial x\|_{x=l_{p,-}} = -\kappa_{\text{eff,s}} \partial \Phi_2 / \partial x\|_{x=l_{p,+}}$ $\partial \Phi_1 / \partial x\|_{x=0} = -I / \sigma_{\text{eff,p}}$
	3	$\sigma_{\text{eff,p}} \partial^2 \Phi_1 / \partial x^2 = a_p F j_p$	and $\quad -\sigma_{\text{eff,p}} \partial \Phi_1 / \partial x\|_{x=l_p} = 0$
	4	$\partial c_s / \partial t = D_{\text{s,p}} / r^2 \partial / \partial r(r^2 \partial c_s / \partial r)$ initial condition $\quad c_s\|_{t=0} = 0.5c_{s,\max,p}$	$\partial c_s / \partial r\|_{r=0} = 0$ and $j_p = -D_{\text{s,p}} \partial c_s / \partial r\|_{r=R_p}$
Separator	5	$\epsilon_s \partial c / \partial t = D_{\text{eff,s}} \partial^2 c / \partial x^2$	$-D_{\text{eff,p}} \partial c / \partial x\|_{x=l_{p,-}} = -D_{\text{eff,s}} \partial c / \partial x\|_{x=l_{p,+}}$ and $-D_{\text{eff,s}} \partial c / \partial x\|_{x=l_p+l_{s,-}} = -D_{\text{eff,n}} \partial c / \partial x\|_{x=l_p+l_{s,+}}$
	6	$I = -\kappa_{\text{eff,s}} \partial \Phi_2 / \partial x + 2\kappa_{\text{eff,s}} RT / F(1 - t_+)\partial \ln c / \partial x$	$-\kappa_{\text{eff,p}} \partial \Phi_2 / \partial x\|_{x=l_{p,-}} = -\kappa_{\text{eff,s}} \partial \Phi_2 / \partial x\|_{x=l_{p,+}}$ and $-\kappa_{\text{eff,s}} \partial \Phi_2 / \partial x\|_{x=l_p+l_{s,-}} = -\kappa_{\text{eff,n}} \partial \Phi_2 / \partial x\|_{x=l_p+l_{s,+}}$
Negative electrode	7	$\epsilon_n \partial c / \partial t = D_{\text{eff,n}} \partial^2 c / \partial x^2 + a_n(1 - t_+)j_n$ initial condition $\quad c\|_{t=0} = c_0$	$-D_{\text{eff,s}} \partial c / \partial x\|_{x=l_p+l_{s,-}} = -D_{\text{eff,n}} \partial c / \partial x\|_{x=l_p+l_{s,+}}$ and $-D_{\text{eff,n}} \partial c / \partial x\|_{x=l_p+l_s+l_n} = 0$
	8	$-\sigma_{\text{eff,n}} \partial \Phi_1 / \partial x - \kappa_{\text{eff,n}} \partial \Phi_2 / \partial x + 2\kappa_{\text{eff,n}} RT / F(1 - t_+)\partial \ln c / \partial x = I$	$-\kappa_{\text{eff,s}} \partial \Phi_2 / \partial x\|_{x=l_p+l_{s,-}} = -\kappa_{\text{eff,n}} \partial \Phi_2 / \partial x\|_{x=l_p+l_{s,+}}$ and $\quad \Phi_2\|_{x=l_p+l_s+l_n} = 0$
	9	$\sigma_{\text{eff,n}} \partial^2 \Phi_1 / \partial x^2 = a_n F j_n$	$-\sigma_{\text{eff,n}} \partial \Phi_1 / \partial x\|_{x=l_p+l_s} = 0$ and $\quad \partial \Phi_1 / \partial x\|_{x=l_p+l_s+l_n} = -I / \sigma_{\text{eff,n}}$
	10	$\partial c_s / \partial t = D_{\text{s,n}} / r^2 \partial / \partial r(r^2 \partial c_s / \partial r)$ initial condition $\quad c_s\|_{t=0} = 0.85c_{s,\max,n}$	$\partial c_s / \partial r\|_{r=0} = 0$ and $j_n = -D_{\text{s,n}} \partial c_s / \partial r\|_{r=R_n}$

$$\frac{\partial C}{\partial \tau} = \epsilon_p^{\text{bruggp-1}} \frac{\partial^2 C}{\partial X^2} + J_p \qquad [5]$$

$$\frac{\partial C}{\partial \tau} = \epsilon_s^{\text{bruggs-1}} \frac{\partial^2 C}{\partial X^2} \qquad [6]$$

$$\frac{\partial C}{\partial \tau} = \epsilon_n^{\text{bruggn-1}} \frac{\partial^2 C}{\partial X^2} + J_n \qquad [7]$$

where the dimensionless variables are $\tau = (D/L^2)t$, $C = (c/c_0)$, $X = x/L$ with the dimensionless groups $J_p = [L^2(1 - t_+)/c_0 D\epsilon_p] \times (I/Fl_p)$ and $J_n = L^2(1 - t_+)/c_0 D\epsilon_n (I/Fl_n)$ where $L = l_p + l_s + l_n$.

The electrolyte concentration can be volume averaged over the respective region as follows

$$C_{\text{ave}}^{\text{cathode}} = \frac{1}{L_p} \int_0^{L_p} C dX, \quad C_{\text{ave}} = \frac{1}{L_s} \int_{L_p}^{L_p+L_s} C dX, \quad \text{and}$$

$$C_{\text{ave}}^{\text{anode}} = \frac{1}{L_n} \int_{L_n+L_s}^{L_p+L_s+L_n} C dX \qquad [8]$$

where $L_p = l_p/L$, $L_s = l_s/L$, and $L_n = l_n/L$. Applying Eq. 8 to the governing equations (Eq. 5-7) yield

$$\frac{dC_{\text{ave}}^{\text{cathode}}}{d\tau} = \frac{\epsilon_p^{\text{bruggp-1}}}{L_p} \left. \left(\frac{dC}{dX}\right)\right|_{X=l_p} + J_p \qquad [9]$$

$$\frac{dC_{\text{ave}}}{d\tau} = \frac{\epsilon_s^{\text{bruggs-1}}}{L_s} \left[\left. \left(\frac{dC}{dX}\right)\right|_{X=l_p+l_s} - \left. \left(\frac{dC}{dX}\right)\right|_{X=l_p} \right] \qquad [10]$$

$$\frac{dC_{\text{ave}}^{\text{anode}}}{d\tau} = \frac{-\epsilon_n^{\text{bruggn-1}}}{L_n} \left. \left(\frac{dC}{dX}\right)\right|_{X=l_p+l_s} + J_n \qquad [11]$$

Note that Eq. 9-11 are ordinary differential equations (ODE) in time as opposed to the original model equations (Eq. 5-7), which are partial differential equations (PDE). Equations 9-11 are exact and as good as the original model equations. Hence, order reduction can be done easily. However, to solve Eq. 9-11, we need to know what the concentration derivatives (flux) are at the two interfaces $x = l_p$ and $x = l_p + l_s$. This is where various approximations come into the picture. By assuming the concentration profile to be a parabolic profile, fluxes at the interfaces can be approximated and Eq. 9-11 are converted as (for $\text{brugg}_p = \text{brugg}_s = \text{brugg}_n = 4$)

Table II. Expressions used in the lithium-ion battery model given by Table I.

$\kappa_{\text{eff,i}} = \epsilon_i^{\text{bruggi}}(4.1253 \times 10^{-2} + 5.007 \times 10^{-4}c - 4.7212 \times 10^{-7}c^2 + 1.5094 \times 10^{-10}c^3 - 1.6018 \times 10^{-14}c^4), \quad \text{i = p, s, n}$

$\sigma_{\text{eff,i}} = \sigma_i(1 - \epsilon_i - \epsilon_{f,i}), \quad \text{i = p, n}$

$D_{\text{eff,i}} = D\epsilon_i^{\text{bruggi}}, \quad \text{i = p, s, n}$

$a_i = 3/R_i(1 - \epsilon_i - \epsilon_{f,i}), \quad \text{i = p, n}$

$j_p = 2k_p(c_{s,\max,p} - c_{s,p}\|_{r=R_p})^{0.5}c_{s,p}\|_{r=R_p}^{0.5}c^{0.5} \sinh[0.5F/RT(\Phi_1 - \Phi_2 - U_p)]$

$U_p = -4.656 + 88.669\theta_p^2 - 401.119\theta_p^4 + 342.909\theta_p^6 - 462.471\theta_p^8 + 433.434\theta_p^{10}/-1.0 + 18.933\theta_p^2 - 79.532\theta_p^4 + 37.311\theta_p^6 - 73.083\theta_p^8 + 95.96\theta_p^{10}$

where $\theta_p = c_{s,p}\|_{r=R_p}/c_{s,p,\max}$

$j_n = 2k_n(c_{s,\max,n} - c_{s,n}\|_{r=R_n})^{0.5}c_{s,n}\|_{r=R_n}^{0.5}c^{0.5} \sinh[0.5F/RT(\Phi_1 - \Phi_2 - U_n + FR_{\text{SEI}}j_n)]$

$U_n = 0.7222 + 0.1387\theta_n + 0.029\theta_n^{0.5} - 0.0172/\theta_n + 0.0019/\theta_n^{1.5} + 0.2808 \exp(0.90 - 15\theta_n) - 0.7984 \exp(0.4465\theta_n - 0.4108)$

where $\theta_n = c_{s,n}\|_{r=R_n}/c_{s,n,\max}$

$$\frac{dC_{\text{ave}}}{dt} = \frac{-6\epsilon_s^3(2C_{\text{ave}} - C_1 - C_3)}{L_s^2} \qquad [12]$$

At the positive electrode, the governing equation for $C_{\text{ave}}^{\text{cathode}}$ is given by

$$\frac{dC_{\text{ave}}^{\text{cathode}}}{dt} = \frac{3\epsilon_p^3(C_1 - C_{\text{ave}}^{\text{cathode}})}{L_p^2} + J_p \qquad [13]$$

At the negative electrode, the governing equation for $C_{\text{ave}}^{\text{anode}}$ is given by

$$\frac{dC_{\text{ave}}^{\text{anode}}}{dt} = \frac{3\epsilon_n^3(C_3 - C_{\text{ave}}^{\text{anode}})}{L_n^2}\frac{(1 - L_p - L_s)}{L_n} + J_n \qquad [14]$$

where

$$C_1 = \frac{3\epsilon_p^4 C_{\text{ave}}^{\text{cathode}} L_s + 6\epsilon_s^4 L_p C_{\text{ave}} - 2\epsilon_s^4 L_p C_3}{3\epsilon_p^4 L_s + 4\epsilon_s^4 L_p} \qquad [15]$$

model is able to predict with no loss in accuracy compared to the rigorous numerical solution using the governing equation for electrolyte concentration in the three regions.

Simplifying lithium-ion battery models without compromising accuracy.— For the simple case shown above, the parabolic profile was used. For lithium-ion battery models, this approach is not the optimized approach. Any dependent variable can be approximated by

$$y(x,t) = \sum_{i=0}^{N_1} a_i(t)\xi_i(x) \qquad [17]$$

where $y(x,t)$ is the dependent variable of interest, $a_i(t)$ is a time-varying coefficient that needs to be determined and $\xi_i(x)$ is a space-dependent function. The function $\xi_i(x)$ can be chosen based on mathematical intuition, experience, and research and can take one of the following forms or a combination of them: linear form (x, $1/x$, etc.), nonlinear form ($\exp(x)$, $\ln(x)$, etc.), trigonometric form [$\sin(x)$, $\sinh(x)$, etc.]. Clearly, as we keep increasing N_1 in Eq. 17,

$$C_3 = \frac{-2\epsilon_s^4 L_n \epsilon_p^4 C_{\text{ave}}^{\text{cathode}} L_s + 4\epsilon_s^8 L_n L_p C_{\text{ave}} + 6\epsilon_s^4 L_n C_{\text{ave}} L_s \epsilon_p^4 + 3\epsilon_n^4 C_{\text{ave}}^{\text{anode}} L_s^2 \epsilon_p^4 + 4\epsilon_s^4 C_{\text{ave}}^{\text{anode}} L_s \epsilon_s^4 L_p}{4\epsilon_s^8 L_n L_p + 4\epsilon_s^4 L_n L_s \epsilon_p^4 + 3\epsilon_n^4 L_s^2 \epsilon_p^4 + 4\epsilon_n^4 L_s \epsilon_s^4 L_p} \qquad [16]$$

More details about finding the constants are illustrated elsewhere for solid-phase diffusion approximations.[18] Note that Eq. 12-14 can be solved exactly (linear equations) to obtain the transient response of the model equations. The accuracy of the reduced-order equations (Eq. 12-14) depends on the system parameters and the complexity of the original model equations. This is a very simple model, and hence, a parabolic profile approximation is sufficient for rates up to $1C$ rate of discharge. Adding more terms to the polynomial profiles improves accuracy, but at the cost of higher computation costs, higher number of equations and needs more work in deriving the reduced-order equations. The method proposed here differs from standard collocation procedures in a subtle manner because we do physics-based averaging and volume averaging on physical variables first.

The simplified model now has three ordinary differential equations (which are initial value problems). Figure 2 gives a comparison of the predictive capability of the simplified model for predicting the electrolyte concentration. It can be seen that the simplified

standard collocation procedures will converge and yield accurate results. The objective is to not to minimize N_1 for a particular variable. The objective is to minimize the total number of differential algebraic equations (DAEs) that result from equations similar to Eq. 17 for all the dependent variables in all the regions to predict the discharge curves accurately (i.e., ΣN_i). This is obtained by combining standard collocation schemes with volume averaging, Liapunov–Schmidt technique, perturbation, Green's function theory, etc. The method needed to simplify each dependent variable in a particular region will be communicated later.

The system of partial differential equations (PDE) shown in Table I form the core of governing equations for battery simulation for a $LiCoO_2$ (positive electrode), LiC_6 (negative electrode) based system. Suppose, we discretize the positive electrode, separator, and negative electrode into 100 equally spaced node points in linear length scale, i.e., in x, the positive electrode now has 100 differential equations for the electrolyte concentration, 100 algebraic equations

Table III. Parameters used for the simulation ($LiCoO_2$ and LiC_6 system).

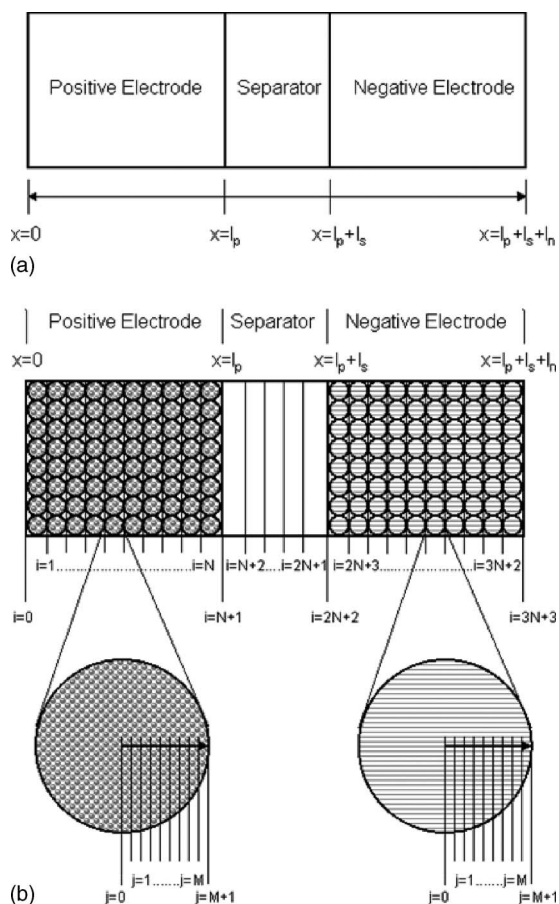| Symbol	Unit	Positive electrode	Separator	Negative electrode
σ_i	S/m	100		100
$\epsilon_{f,i}$		0.025		0.0326
ϵ_i		0.385	0.724	0.485
Brugg			4	
$D_{s,i}$	m^2/s	1.0×10^{-14}		3.9×10^{-14}
D	m^2/s		7.5×10^{-10}	
k_i	mol/(s m^2)/(mol/m^3)$^{1+\alpha a,i}$	2.334×10^{-11}		5.0307×10^{-11}
$c_{s,i,max}$	mol/m^3	51554		30555
$c_{s,i0}$	mol/m^3	0.4955×51554		0.8551×30555
c_0	mol/m^3		1000	
R_p	m	2.0×10^{-6}		2.0×10^{-6}
l_i	m	80×10^{-6}	25×10^{-6}	88×10^{-6}
R_{SEI}	Ω m^2			0.0
t_+			0.363	
F	C/mol		96487	
R	J/(mol K)		8.314	
T	K		298.15	

Figure 1. (a) Schematic illustration of lithium ion cell sandwich and (b) lithium-ion battery stencil (rigorous numeric model).

for the electrolyte potential (potential in the electrolyte phase), and 100 algebraic equations for the solid-phase potential. If we take 20 node points in r for the solid particles present in every node point in x, then for the solid phase concentration we have $1 \times 100 \times 20$ differential equations. Thus, for a single porous electrode (say for
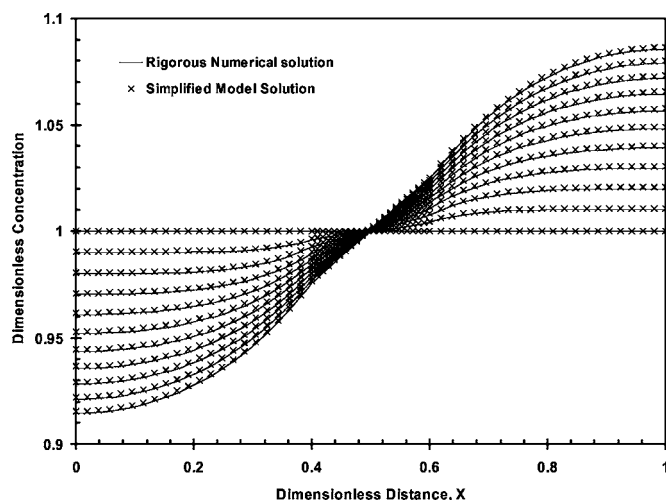

Figure 2. Variation of dimensionless concentration plotted as a function of dimensionless cell distance X for various times. There is good agreement between the rigorous numerical model and the reformulated simplified model for the simple case of uniform current distribution (Eq. 1-3 and Eq. 12-14).
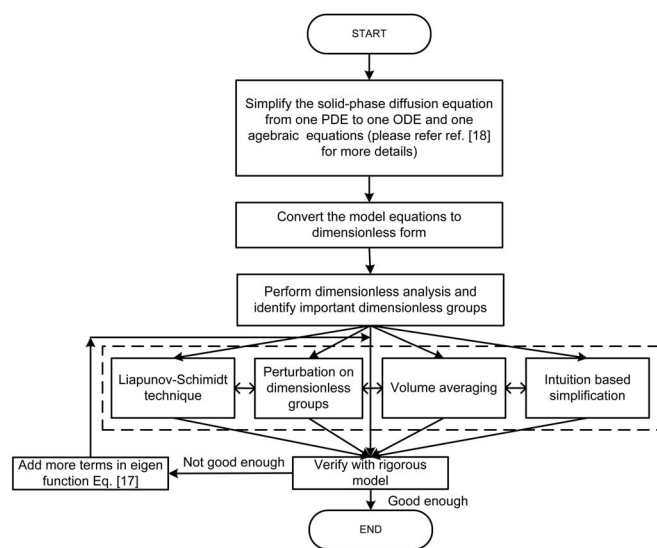

Figure 3. Computation scheme for model simplification.

positive electrode), we have 2300 DAEs. Following the same number of node points in x, the separator now has 100 differential equations for the electrolyte concentration and 100 algebraic equations for the electrolyte phase potential. The negative electrode is discretized similar to the positive electrode and has a total of $3 \times 100 + 1 \times 100 \times 20 = 2300$ DAEs to solve. Thus, the number of differential algebraic equations to be solved for the rigorous model is $3 \times 100 + 1 \times 100 \times 20 + 2 \times 100 + 3 \times 100 + 1 \times 100 \times 20 = 4800$ DAEs. By using parabolic profile and other approximations, solid-phase diffusion can be approximated and the number of DAEs are reduced to 302 DAEs, as shown in Ref. 18.

By using the approximations discussed in this paper, we are able to predict the discharge curves accurately with just 49 DAEs. Note that 49 DAEs are needed for matching for all the intrinsic variables. With our approach, we can choose to go "approximate" in the intrinsic variables and solve only discharge curves accurately with only 27 DAEs. More information regarding model simplification is outlined in Fig. 3, and each step in the flowchart will be published as a separate paper in the future.

These models take 30 s to 2 min to run in the Maple environment using a DAE solver called Besirk.[19] A variant of the same model runs in 85 ms in Fortran environment to predict an entire discharge curve (1.7 GHz processor and 1 GB RAM). An executable code that predicts the discharge behavior in real time is available on request from the corresponding author. We have tested our simplified models for rates up to $2C$ and are in the process of testing for rates up to $50C$ (for higher rates solid-phase approximation needs to be redefined).

Discussion

Discharge behavior of lithium-ion batteries is the prime goal of the simulation performed in this paper. Figure 4 gives the discharge curve for $1C$ and $1/2C$ rates of discharge. It can be seen that for these rates of discharge the simplified model compares very well to the rigorous numeric model. The merit of the approach is evident when comparing the number of governing equations that are solved. The simplified model specifies 49 DAEs as opposed to 302 DAEs for the rigorous code. It is also noteworthy that 302 is the minimum number of DAEs required for a converged finite difference solution. The simplified model for all practical situations (rates of discharge) uses a maximum of 49 specified equations for a converged solution, which compares very well, even with 302 DAEs based finite difference code.
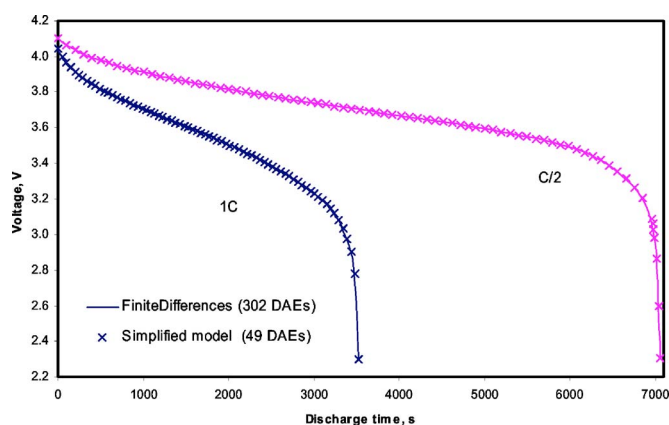
Figure 4. (Color online) Discharge curves for 1*C* and 0.5*C* rate comparing the rigorous numerical model and the reformulated simplified model. Good agreement is seen between the two.
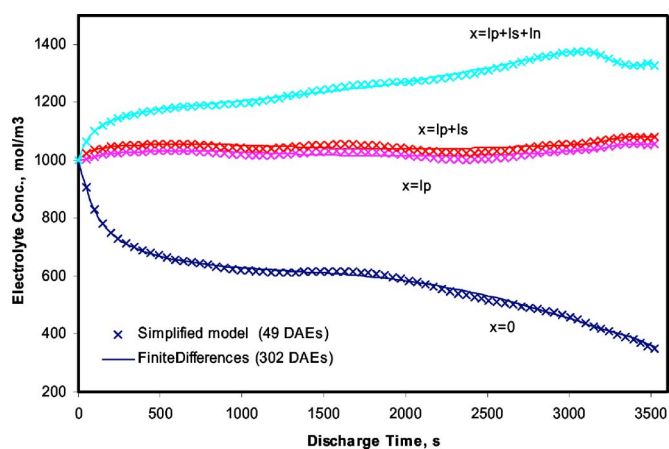

Figure 7. (Color online) Overpotential η is plotted as a function of time of discharge at different interfaces comparing the reformulated simplified and rigorous numerical models. Good agreement is seen between the two models.

Figure 5. (Color online) Solution phase concentration profiles for 1*C* rate at different interfaces comparing the rigorous numerical model and the reformulated simplified model. There is good agreement between the two models.
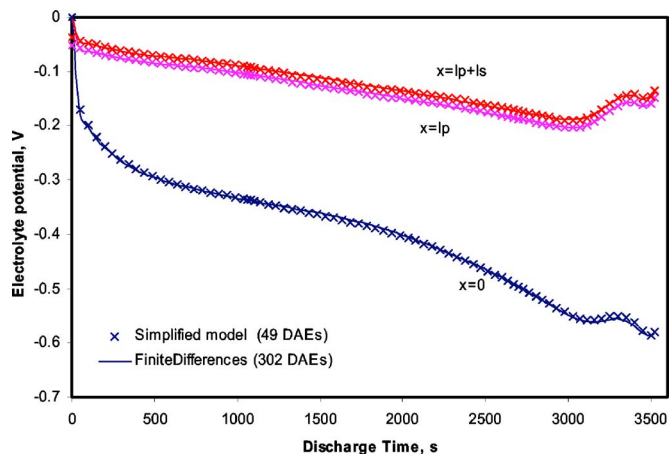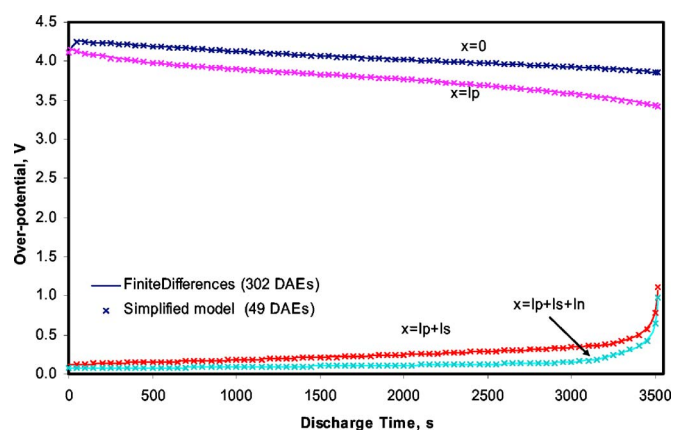

Figure 6. (Color online) Solution phase potential at different interfaces comparing the reformulated, simplified, and rigorous numerical models are plotted for a 1*C* rate of discharge. There is good agreement between the two models.

The simplified model also predicts the intrinsic variables accurately. The intrinsic variables, namely, overpotential (η), solution phase potential (Φ_2), solid-phase potential (Φ_1), and electrolyte concentration (Fig. 5) determined by the simplified model, are plotted and compared to a rigorous finite difference code. The interfaces are the positive electrode-current collector junction ($x = 0$), positive electrode-separator (electrolyte) junction ($x = l_p$), separator-negative electrode junction ($x = l_p + l_s$), and the negative electrode-current collector junction ($x = l_p + l_s + l_n$). Figure 6 shows the comparison of solution phase potential at various interfaces for both simplified and rigorous numeric models. It is seen that the changes in solution phase potential at the current collector-negative electrode junction and negative electrode-separator junction are predicted well by the simplified model. Figure 7 shows the comparison of overpotential at various interfaces. It has been clearly seen that the simplified model, although saving computational time, does not compromise physics of the system.

The form of eigenfunction in Eq. 17 for each dependent variable in a particular region determines the efficiency of the simplified code. More details regarding eigenfunctions for a particular dependent variable in a particular region will be discussed in future publications.

Conclusion

This paper presents an efficient approach to simulate discharge behavior of lithium-ion batteries in real time (milliseconds). Only preliminary results are discussed in this paper, and future publications will discuss the math involved in simplifying these models in more depth. Since the model simplification method is demonstrated using low to moderate rates of discharge due to mass transport limitations, the simplified model presented is also valid only under these circumstances. The method proposed is also expected to be valid for all other Li-ion battery chemistries and other electrochemical power sources, such as PEM fuel cells, nickel-metal hydride batteries, etc. The method developed has significance in hybrid modeling and control, parameter estimation from experimental data (capacity fade and lifetime prediction), etc.

Acknowledgment

List of Symbols

a_i specific surface area of electrode i (i = p, n), m^2/m^3

brugg$_i$ Bruggman coefficient of region i (i = p, s, n)

c electrolyte concentration, mol/m^3

c_0 initial electrolyte concentration, mol/m^3

$c_{s,i}$ concentration of lithium ions in the intercalation particle of electrode i (i = p, n), mol/m^3

$c_{s,i,0}$ initial concentration of lithium ions in the intercalation particle of electrode i (i = p, n), mol/m^3

$c_{s,i,max}$ maximum concentration of lithium ions in the intercalation particle of electrode i (i = p, n), mol/m^3

D electrolyte diffusion coefficient, m^2/s

$D_{s,i}$ lithium ion diffusion coefficient in the intercalation particle of electrode i (i = p, n), m^2/s

F Faraday's constant, C/mol

I applied current density, A/cm^2

i_1 solid phase current density, A/m^2

i_2 solution phase current density, A/m^2

$i_{s,0}$ exchange current density for the solvent reduction reaction, A/m^2

j_s solvent reduction current density, mol/m^{2}s

j_i wall flux of Li$^+$ on the intercalation particle of electrode i (i = n, p), mol/m^{2}s

k_i intercalation/deintercalation reaction rate constant of electrode i (i = p, n), mol/(mol/m^3)$^{1.5}$

l_i thickness of region i (i = p, s, n), m

M_s molar weight of the solvent reaction product, g/mol

n   negative electrode

p   positive electrode

r radial coordinate, m

R universal gas constant, J/(mol K)

R_{SEI} initial SEI layer resistance at the negative electrode, Ω m^2

R_i radius of the intercalation particle of electrode i (i = p, n), m

s   separator

t_+ Li$^+$ transference number in the electrolyte

T absolute temperature, K

U_i open circuit potential of electrode i (i = p, n), V

U_s standard potential of the solvent reduction reaction, V

x spatial coordinate, m

δ thickness of the solvent reduction product film, m

δ_0 initial thickness of the solvent reduction product film, m

ϵ_i

$\epsilon_{f,i}$ porosity of region i (i = p, s, n) / volume fraction of fillers of electrode i (i = p, n)

θ_i dimensionless concentration of lithium ions in the intercalation particle of electrode i ($\theta_i = c_{s,i}/c_{s,i,max}$)

κ ionic conductivity of the electrolyte, S/m

$\kappa_{eff,i}$ effective ionic conductivity of the electrolyte in region i (i = p, s, n), S/m

ρ_s density of the solvent reduction product film, g/m^3

σ_i electronic conductivity of the solid phase of electrode i (i = p, n), S/m

$\sigma_{eff,i}$ effective electronic conductivity of the solid phase of electrode i (i = p, n), S/m

Φ_1 solid phase potential, V

Φ_2 electrolyte phase potential, V

References

1. M. Doyle, T. F. Fuller, and J. Newman, *J. Electrochem. Soc.*, **140**, 1526 (1993).
2. J. Newman and W. Tiedmann, *AIChE J.*, **21**, 25 (1975).
3. T. F. Fuller, M. Doyle, and J. Newman, *J. Electrochem. Soc.*, **141**, 982 (1994).
4. T. F. Fuller, M. Doyle, and J. Newman, *J. Electrochem. Soc.*, **141**, 1 (1994).
5. M. Doyle, J. Newman, A. S. Gozdz, C. N. Schmutz, and J. M. Tarascon, *J. Electrochem. Soc.*, **143**, 1890 (1996).
6. K. E. Thomas and J. Newman, *J. Electrochem. Soc.*, **150**, A176 (2003).
7. P. Arora, M. Doyle, A. S. Gozdz, R. E. White, and J. Newman, *J. Power Sources*, **88**, 219 (2000).
8. P. Ramadass, B. Haran, R. E. White, and B. N. Popov, *J. Power Sources*, **123**, 230 (2003).
9. P. Ramadass, B. Haran, P. M. Gomadam, R. E. White, and B. N. Popov, *J. Electrochem. Soc.*, **151**, A196 (2004).
10. G. Ning, R. E. White, and B. N. Popov, *Electrochim. Acta*, **51**, 2012 (2006).
11. G. G. Botte, V. R. Subramanian, and R. E. White, *Electrochim. Acta*, **45**, 2595 (2000).
12. P. M. Gomadam, J. W. Weidner, R. A. Dougal, and R. E. White, *J. Power Sources*, **110**, 267 (2002).
13. S. Santhanagopalan, Q. Guo, P. Ramadass, and R. E. White, *J. Power Sources*, **156**, 620 (2006).
14. V. Balakotaiah and S. Chakraborty, *Chem. Eng. Sci.*, **58**, 4769 (2003).
15. V. Balakotaiah and H-C. Chang, *SIAM J. Appl. Math.*, **63**, 1231 (2003).
16. F. A. Howes and S. Whitaker, *Chem. Eng. Sci.*, **40**, 1387 (1985).
17. M. Golubitky and D. G. Schaeffer, *Singularities and Groups in Bifurcation Theory*, Vol. 1, Springer-Verlag, Berlin (1984).
18. V. R. Subramanian, V. D. Diwakar, and D. Tapriyal, *J. Electrochem. Soc.*, **152**, A2002 (2005).
19. http://people.clarkson.edu/~chengweb/faculty/taylor/ (accessed August 2007).